UNIVERSITY OF CAMBRIDGE
Department of Engineering

Influence of Boussinesq coefficient on Unsteady Flood Modelling with Shallow Water Equations

Author Name: Yasir Choudhry
Supervisor: Dr Liang
Date: 26/05/2020

I hereby declare that, except where specifically indicated, the work submitted herin is my own original work.

Signed yasir. *date* 26.05.20

UNIVERSITY OF CAMBRIDGE
DEPARTMENT OF ENGINEERING

Project Final Report: Influence of Boussinesq coefficient on Unsteady Flood Modelling with Shallow Water Equations

Yasir Choudhry

Supervisor: Dr Liang

Pembroke College

May 2020

Technical Abstract

The modelling of flooding events is incredibly important and often forms the basis of guidance given by governments. It is especially important to understand this effect when it comes to dam-break floods which have caused devastation in the past. Many dams exist near or upstream of urban areas and therefore the potential damage that a flood wave resulting from a collapse of the dam could be catastrophic.

When modelling these types of floods, the shallow water equations are usually employed. Which are a depth-integrated version of the Navier-Stokes equations. The model used in this project makes uses of these equations alongside the TVD-MacCormack explicit finite difference scheme.

The Boussinesq coefficient is also knows as the momentum correction factor for non-uniform vertical velocity profile. It is a measure of the degree to which the velocity distribution is not uniform (i.e. there exists a variation such that the flow at some depths is slower/faster than another). This value has been theoretically and experimentally found to be almost always very close to unity in the flow conditions that would be seen in a dam-break event. However, it is often modified to stabilize the program for other computational schemes such as ADI (Alternating Direction Implicit).

Two different scenarios were tested, both involving flooding after a dam break.

First, the result of changing the Bousinesq coefficient was tested with a study of the Malpasset dam collapse scenario. This was a real-life event for which data is available supplemented by further data from a scale model. Several tests were run with a range of values for the coefficient. The data from these tests including maximum water level and time taken for the flood wave to arrive was extracted at several points. This was then compared to the findings from the real-life/model data. The effect of changing the Boussinesq coefficient was found to be not very significant but a general trend of a slower moving flood wave in the upstream section due to lower values of the coefficient was observed.

The second test was based on simulating a flood in the Toce River valley. The trends observed were similar to the first test but also showed an expected increase in maximum depth when the Boussinesq coefficient was decreased. Comparisons with the expected data from a scale model indicated values closer to the actual values of the coefficient (near 1) showed more unreasonable values tended to result in less accurately predicted maximum depths.

This ties in with previous research suggesting that when bed friction is not significant, increasing the Boussinesq coefficient leads to a faster moving flood wave and vice versa. Which, through conservation of mass, explains the smaller maximum water depth.

Table of Contents

List of Figures

1 Introduction

1.1 Background

Damn break events are catastrophic and often result in significant loss of life. Dams are designed to restrict the flow of water downstream and have varied uses from irrigation and agriculture to electricity generation and even navigation. Many dams have a significant reservoir upstream which is often a cause for concern. If the dam was to break (either a leak leading to eventual collapse or a more sudden structural failure) the resulting flow of water can cause serious harm.

The UK itself has over 500[1] large dams and many of these dams hold the potential to cause a life-threatening flood if they were to fail. A recent scare occurred in Whaley Bridge, Derbyshire when, after several days of unusually heavy rain, the Toddbrook Reservoir was damaged[2] requiring the evacuation of 1,500 people and a military assisted operation involving 530 tonnes of airlifted aggregate. This is an example of how crucial it is to be able to model dam break floods accurately.

Figure 1: Chinook helicopter used to airlift aggregate on to the damaged section of the dam near Whaley Bridge

The Malpasset dam break (which is one of the events considered in this report) has been the subject of extensive studies and models in the past. It was located in the southern region of France 7km north of the town of Frejus and its collapse resulted in hundreds of casualties and millions of euros of damage due to the dam-break wave and the subsequent flooding it caused. The ability to accurately predict this type of flooding and to be able to assess the potential damage that such events could cause in other situations or other dam-break events is important. Since there is extensive data available for this event, a flooding simulation can be compared to what was observed and recorded during the actual event itself. There have been several studies where an appropriately scaled model of the dam was constructed and the data from that test also provides a useful comparison.

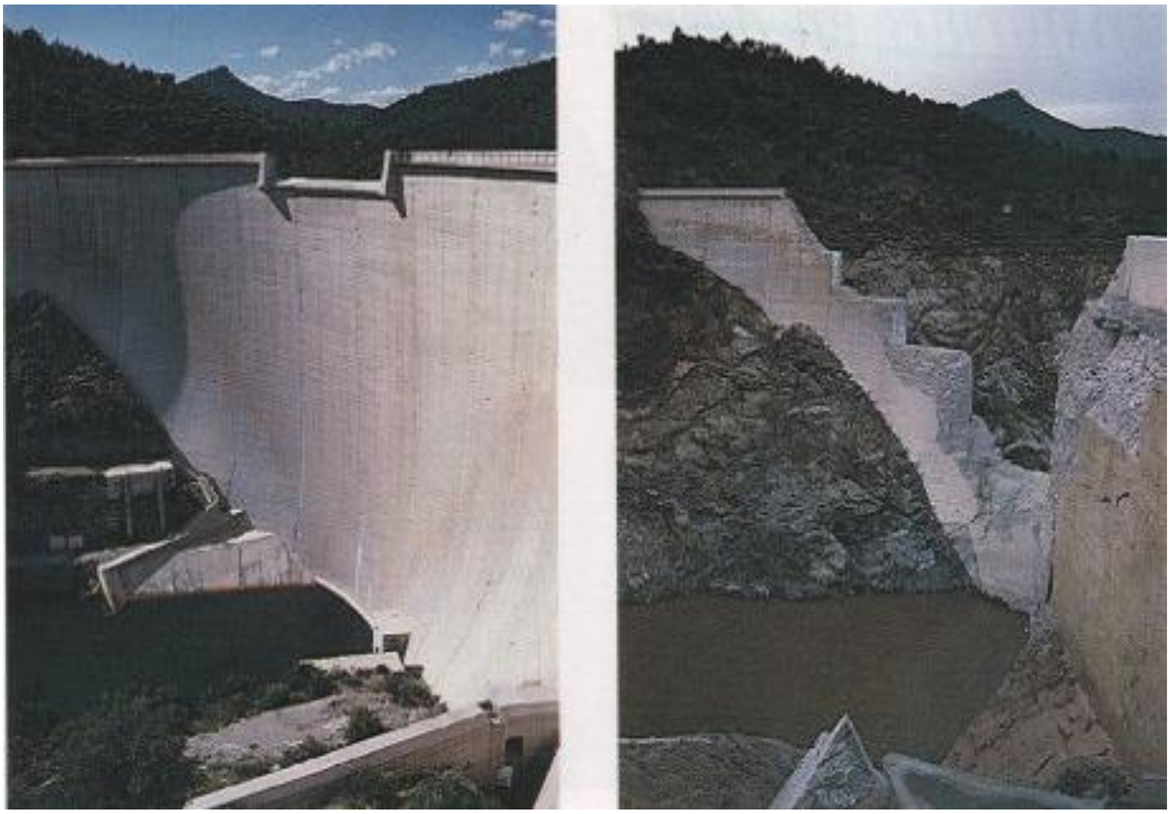

Figure 2: Malpasset Dam before and after collapse

In order to supplement this, there is also data from a scale model of the Toce River valley in Italy. Although there was no actual flood in this location, the data provides a useful comparison to see if trends are consistently observed between models.

In the UK, the EA (Environment Agency) is charged with advising local planning authorities on publishing maps and issuing guidance on what areas are at risk from flooding. 2D modelling is often used to predict flood extents and due to the nature of flooding events 'shock-capturing' models are used which are also able to deal with moving wet/dry boundaries and uneven topographies. These usually have high computational cost compared to alternative models based on the ADI (alternating direction implicit) algorithm (which are not very accurate for rapidly varying flows).

A program, written by Dr Liang, based on the TVD-MacCormack scheme using the shallow water equations is used instead which has been shown to work well in both hypothetical and realistic configurations.[6]

1.2 Aim

This type of flooding simulation is run based on the shallow water equations. Many different commercial packages exist to simulate this type of unsteady flooding, but they are often 'closed source' and many parameters cannot be changed. One parameter that plays a crucial role is the Boussinesq coefficient otherwise known as the momentum correction coefficient. This is used to account for the non-uniformity in the velocity distribution. For the ADI scheme, which is used by several commercial programs[15] the Boussinesq coefficient is often changed to stabilize the program when simulating rapid flows.

The aim of this project is to understand the effect that changes in this coefficient have on flooding simulation and how this changes for different flow conditions and scenarios. It is also important to understand how changes in this coefficient affect the degree to which the result of the simulation closely matches the physical results.

2 Theory

The Boussinesq coefficient is a measure of how uniform the velocity distribution is and when it is at unity the velocity distribution over depth is deemed to be uniform.

It can be defined as:

$$\beta = \frac{\int_{z_b}^{\eta} u^2 dz}{U^2 A}$$

Where:

U: depth-averaged velocity

H: total water column depth

u: flow velocity at a given point

z: vertical coordinate

η: water surface elevation above datum

For a logarithmic velocity profile[14] is can be expressed as:

$$\beta = \left(1 + \frac{g}{C^2 \kappa^2}\right)$$

Where:

C: Chezy coefficient

K: Karman's constant

When the value of the Chezy coefficient is increased, the Boussinesq coefficient decreases. This suggest that a decrease in bed roughness leads to an increase in the Boussinesq coefficient.

This coefficient was first proposed by J.V. Boussinesq in 1877[3] in his original book in hydraulics. In hydraulic jumps for example this coefficient can easily reach as high as 2.5 due to the highly non-uniform velocity profile in such conditions. This has been demonstrated to be the case in previous experiments with a detailed investigation into them[4].

Theoretically, its value should always be larger than 1 as both uniform velocity distribution and conventional and non-conventional distributions would result in a calculated coefficient equal to or slightly greater than one.

In turbulent open channel flows the velocity distribution is said to be approximately given by the Prandtl power law.

$$\frac{v}{V_{max}} = \left(\frac{y}{d}\right)^{1/N}$$

Where:

y: distance from the free surface

d: water depth in the channel

N: a factor that can vary

N can vary from about 4 to 12 depending on the conditions of the channel such as the shape of the cross section and the boundary friction.[5]

This can be used to get an idea for the range on values that the boussinesq coefficient could take.

$$V = \frac{1}{A}\int_A vdA$$

Assuming a wide channel the expression becomes:

$$V = \frac{1}{d}\int_0^d vdy$$

$$\beta = \frac{1}{V^2 d}\int_0^d v^2 dy$$

Taking v as:

$$v = const \times y^{1/N}$$

Resulting in:

$$\int_0^d v dy = \frac{const}{\frac{1}{N}+1} \times y^{(1/N+1)} \text{ and } \int_0^d v^2 dy = \frac{const^2}{\frac{2}{N}+1} \times y^{(2/N+1)}$$

And the following expression for the Boussinesq coefficient:

$$\beta = \frac{\left(\frac{1}{N}+1\right)^2}{\left(\frac{2}{N}+1\right)}$$

Using the previously suggested 'N' values (4 to 12), this results in a range from 1.042 to 1.006 which suggests that the value is typically very close to unity. But this may not be the case if the wide channel assumption is not made.

The momentum equation is usually written as:

$$\rho\beta Q(V_2 - V_1) = \left(\frac{1}{2}\rho g d_1^2 B_1\right) - \left(\frac{1}{2}\rho g d_2^2 B_2\right)$$

Where B is the channel width and Q is discharge.

If the velocity distribution is not uniform it is modified as follows:

$$\rho\beta Q(\beta_1 V_2 - \beta_2 V_1) = \left(\frac{1}{2}\rho g d_1^2 B_1\right) - \left(\frac{1}{2}\rho g d_2^2 B_2\right)$$

By reducing the coefficient the effect of momentum is reduced and therefore inertial forces play a smaller part. If the coefficient was set to zero, the flow would thus be mostly governed by gravity instead and advective acceleration terms ignored.

2.2 Shallow Water Equations

The shallow water equations are obtained by depth-integrating the Navier-Stokes equations on several assumptions like the hydrostatic pressure distribution and small bottom slope. They apply in cases where the horizontal length scale is much greater than the vertical water depth scale. They are applied in a broad range of areas including urban flooding, river hydraulics and Dam-break scenarios. If the viscous forces, Coriolis forces and wind are disregarded, the non-conservative form of the equations can be written as follows: Since dam-break flows are usually of high velocity, they can be considered advection dominated and eddy viscosity terms neglected.

$$\frac{\partial \zeta}{\partial \mathrm{t}} + \frac{\partial q_x}{\partial \mathrm{x}} + \frac{\partial q_y}{\partial \mathrm{y}} = 0 \qquad (1)$$

$$\frac{\partial q_x}{\partial \mathrm{t}} + \frac{\partial \left(\frac{\beta q_x^2}{H}\right)}{\partial \mathrm{x}} + \frac{\partial \left(\frac{\beta q_x q_y}{H}\right)}{\partial \mathrm{y}} = -gH\frac{\partial \zeta}{\partial \mathrm{x}} - \frac{g q_x \sqrt{q_x^2 + q_y^2}}{H^2 C^2} \qquad (2)$$

$$\frac{\partial q_y}{\partial \mathrm{t}} + \frac{\partial \left(\frac{\beta q_y^2}{H}\right)}{\partial \mathrm{y}} + \frac{\partial \left(\frac{\beta q_x q_y}{H}\right)}{\partial \mathrm{x}} = -gH\frac{\partial \zeta}{\partial \mathrm{y}} - \frac{g q_y \sqrt{q_x^2 + q_y^2}}{H^2 C^2} \qquad (3)$$

Where:

H is the total water column depth

C is the Chezy value

ζ is the water surface elevation above datum

q_x and q_y are the discharge per unit width components in the x and y directions

β is the momentum correction factor for non-uniform flow

g is the acceleration due to gravity

3 Program Setup

This section is work already carried out by Dr Liang, Prof Lin and Prof Falconer[6][7]. As the basis for the program through which the testing was done.

3.1 Coordinate system

In order to better capture the site geometry, a curvilinear computational mesh is generated in the (x, y) plane which is mapped on to a uniform rectangular mesh in the (ξ, η) plane. This is done through a Jacobian that does not vary with time as the mesh is fixed throughout the computation. Equations (1,2,3) therefore become (5,6,7).

$$J = \frac{\partial x}{\partial \xi}\frac{\partial y}{\partial \eta} - \frac{\partial x}{\partial \eta}\frac{\partial y}{\partial \xi} \tag{4}$$

$$\frac{\partial(J \cdot \zeta)}{\partial t} + \frac{\partial(q_x \cdot \frac{\partial y}{\partial \eta} - (q_y \cdot \frac{\partial x}{\partial \eta})}{\partial \xi} + \frac{\partial(q_y \cdot \frac{\partial x}{\partial \xi} - (q_x \cdot \frac{\partial y}{\partial \xi})}{\partial \eta} = 0 \tag{5}$$

$$\frac{\partial(J \cdot q_x)}{\partial t} + \frac{\partial\left(\frac{\beta q_x^2}{H} \cdot \frac{\partial y}{\partial \eta} - \frac{\beta q_x q_y}{H} \cdot \frac{\partial x}{\partial \eta}\right)}{\partial \xi} + \frac{\partial\left(\frac{\beta q_x q_y}{H} \cdot \frac{\partial x}{\partial \xi} - \frac{\beta q_x^2}{H} \cdot \frac{\partial y}{\partial \xi}\right)}{\partial \eta}$$

$$= -gH\frac{\partial y}{\partial \eta} \cdot \frac{\partial \zeta}{\partial \xi} + gH\frac{\partial y}{\partial \xi} \cdot \frac{\partial \zeta}{\partial \eta} - J \cdot \frac{g q_x\sqrt{q_x^2 + q_y^2}}{H^2 C^2} \tag{6}$$

$$\frac{\partial(\mathrm{J}\cdot q_{y})}{\partial \mathrm{t}}+\frac{\partial\left(\frac{\beta q_x q_y}{H}\cdot\frac{\partial \mathrm{y}}{\partial \eta}-\frac{\beta q_y^2}{H}\cdot\frac{\partial \mathrm{x}}{\partial \eta}\right)}{\partial \xi}+\frac{\partial\left(\frac{\beta q_y^2}{H}\cdot\frac{\partial \mathrm{x}}{\partial \xi}-\frac{\beta q_x q_y}{H}\cdot\frac{\partial \mathrm{y}}{\partial \xi}\right)}{\partial \eta}$$

$$=+gH\frac{\partial \mathrm{x}}{\partial \eta}\cdot\frac{\partial \zeta}{\partial \xi}-gH\frac{\partial \mathrm{x}}{\partial \xi}\cdot\frac{\partial \zeta}{\partial \eta}-\mathrm{J}\cdot\frac{g q_y\sqrt{q_x^2+q_y^2}}{H^2C^2} \tag{7}$$

3.2 Solving Methods

The equations (5,6,7) are solved after being split in to two sets of one-dimensional equations. This allows for solutions to be found in the ξ and η every time step (with the order reversed every time step to improve accuracy). Therefore, only the variance of the variables in the ξ direction is considered in one set of equations and then η in the other.

For example, only considering the ξ direction:

$$\frac{\partial(\mathrm{J}\cdot\zeta)}{\partial \mathrm{t}}+\frac{\partial(q_x\cdot\frac{\partial \mathrm{y}}{\partial \eta}-(q_y\cdot\frac{\partial \mathrm{x}}{\partial \eta})}{\partial \xi}=0 \tag{8}$$

$$\frac{\partial(\mathrm{J}\cdot q_{x})}{\partial \mathrm{t}}+\frac{\partial\left(\frac{\beta q_x^2}{H}\cdot\frac{\partial \mathrm{y}}{\partial \eta}-\frac{\beta q_x q_y}{H}\cdot\frac{\partial \mathrm{x}}{\partial \eta}\right)}{\partial \xi}=-gH\frac{\partial \mathrm{y}}{\partial \eta}\cdot\frac{\partial \zeta}{\partial \xi}-\mathrm{J}\cdot\frac{g q_x\sqrt{q_x^2+q_y^2}}{H^2C^2} \tag{9}$$

$$\frac{\partial(\mathrm{J}\cdot q_{y})}{\partial \mathrm{t}}+\frac{\partial\left(\frac{\beta q_x q_y}{H}\cdot\frac{\partial \mathrm{y}}{\partial \eta}-\frac{\beta q_y^2}{H}\cdot\frac{\partial \mathrm{x}}{\partial \eta}\right)}{\partial \xi}=gH\frac{\partial \mathrm{x}}{\partial \eta}\cdot\frac{\partial \zeta}{\partial \xi} \tag{10}$$

By reversing the order of the solutions every two consecutive time steps (solutions in the other directions), the accuracy of the predictions can be enhanced and is called an alternating operator-splitting strategy[11].

3.2.1 Mac-TVD and Numerical Scheme

The MacCormack explicit finite difference scheme constitutes the basis of the present numerical method for these two sets of equations, which comprises the predictor and corrector steps. By using this two-stage scheme, the source terms can be easily handled to achieve second-order accuracy, both in time and space. The standard MacCormack scheme has second-order accuracy. It is well known that a second-order scheme gives rise to spurious numerical oscillations close to the sharp gradients in the solution. A fivepoint symmetric TVD term is appended to the corrector step of the MacCormack scheme to prevent non-physical oscillations. The basic principle is to adjust the introduced numerical diffusion so that the second-order accurate MacCormack scheme is deployed where the solution is smooth, while the first-order accurate upwind scheme is deployed where the solution contains sharp gradients to avoid fictitious oscillations. The main advantage of the present TVD scheme is that no characteristic transformation is needed, and hence the computational cost is particularly low. It should be noted that the finite difference and the finite volume methods are equivalent to each other for the present grid structure and numerical scheme. Although the nonconservative form of the SWEs is deployed, i.e., the momentum equations are not expressed in a strict hyperbolic formulation, it is possible for the present scheme to allow for mass and momentum conservation and energy loss near shocks. To ensure that conservation is maintained, the coefficients before the main derivatives, such as $gH\frac{\partial y}{\partial \eta}$ and $gH\frac{\partial x}{\partial \eta}$ in the first right-hand-side terms in Eqs. (9 and 10), need to be approximated by the arithmetic average in the difference direction[12].

Numerical instabilities may develop when the water depth gets very small, due to the presence of water depth in the denominator of several terms in the momentum equations. In particular, the bed friction term will dominate over other terms for small water depths. Using explicit schemes in such cases often leads to unstable oscillations in the computed velocities. To enhance the robustness of the model, the bed friction term is discretized semi-implicitly when the water depth is below a threshold value. Another challenge associated with a dry bed is the determination of the moving boundary, since the wet/dry interface is sometimes not fixed. Wetting and drying checks are performed within each time step in the time marching process. The grid cell is deemed as being dry when the water depth is smaller than a prescribed value. On dry cells, the normal numerical solution of the governing equations is bypassed by directly setting the velocities to zero and leaving the water level unchanged. In the wetting check, the dry cell is included in the wet domain if the nearby water surface elevation is found to be higher than the dry cell's bed elevation. The return of the dry cell into the wet domain is achieved by increasing the water surface position on the dry cell to be slightly higher than the bed elevation. Correspondingly, the same amount of water is decreased from the adjacent wet cell. Care has been taken to ensure a no-flow condition at the wet/dry interface, so that mass balance in the flow is conserved. As required by almost all of the explicit numerical schemes, the time step should be small enough for the computations to satisfy the well-known Courant– Friedrich–Lewy condition, i.e., the Courant number needs to be <1.

4 Malpasset: Setup, Results and Discussion

4.1 Setup

The Malpasset dam was located in southern France upstream of the town of Frejus in the Reyran river valley built between 1952 and 1954 and collapsed in 1959. It was an arch dam with a crest length of 233m and a maximum height of 66.5m. The purpose of the dam was to supply water to the region and provide flood risk management by reducing the potential inundation risk in the Reyran River.

Failure resulted in a flooding wave over 40m high[9] and the release of about 50 million cubic meters of water in the valley which is about 12km long. There were 421 casualties in the town of Frejus and over $70 million in damage.

The water level in the reservoir is initially set to 100m (above sea level) while the rest of the domain is assumed to be initially dry. As the dam is an arch dam, the dam is assumed to break instantly and dam height changed to 56.8m above sea level, which remains constant throughout the simulation. The topography used in this model is based on a digitized map dating back to 1931. After the dam-break in 1959, there were significant changes to the topography thus modern topography is not used. This test therefore involves predicting real life supercritical flow including uneven terrain with a moving wet/dry boundary.

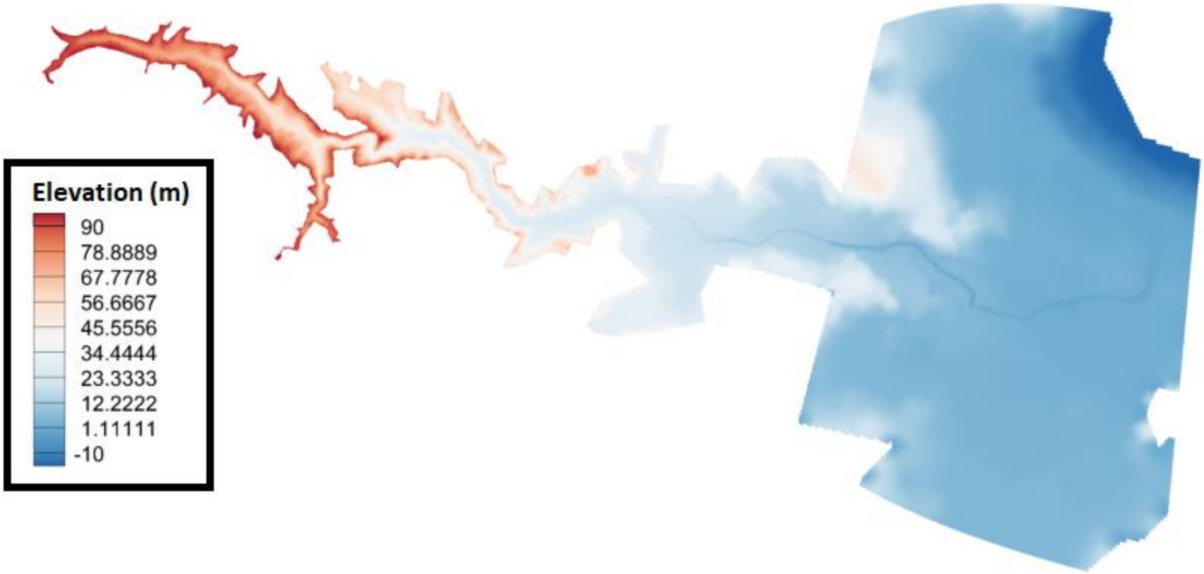

Figure 3: Topography being used of the Malpasset site before the flood

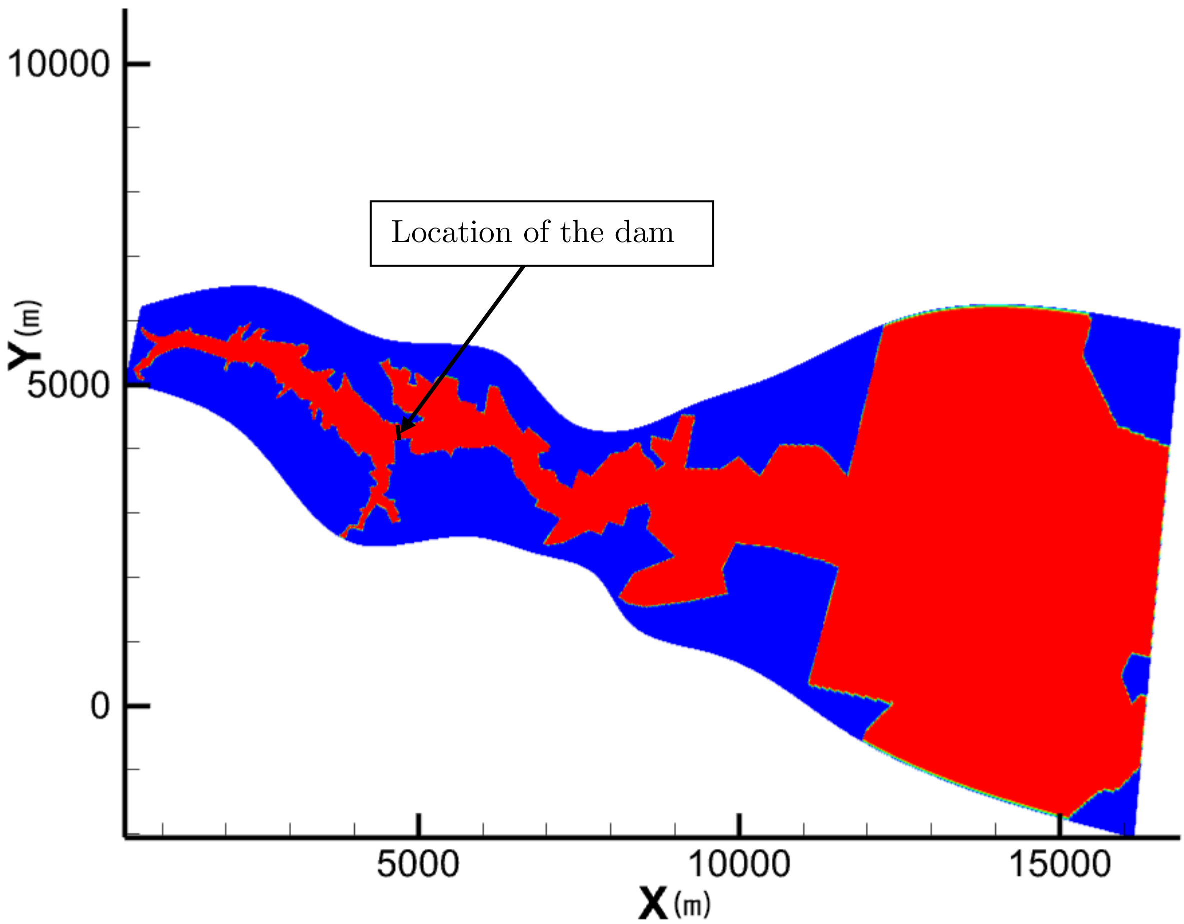

Figure 4: Computational domain of the Malpasset site

A structured mesh is created (outlined in blue in Figure 4) within which some of the mech is 'active' and considered in the simulation (shown as red) while the remaining 'grids' are not considered in the calculations. The grid size varies from about 5m to 50m across the domain due to the variation in the non-uniform and non-orthogonal mesh being used. The mesh size (including non-active grids) is 1092 x 201. This domain stretches from upstream of the dam to the 'sea' and is about 17km 'long' and 8.5km wide at the downstream end. Based on previous research[8], the Manning coefficient is set to $0.033 s/m^{1/3}$ across the whole domain. Initial tests were done with a time step of 0.2s as was used in previously, but later repeated with a time step of 0.1s. The minimum water level at which a cell was considered 'wet' was set to 0.8m. At levels below this the grid cell was deemed dry and the equations bypassed with the velocity set to zero instead.

4.1.1 Existing Data

In 1961 1:400 scale model of the dam was constructed by the French national electric utility company (Electricite de France) in the National Hydraulic and Environment Laboratory to study the dam break flood. The results from this study can be used as a useful comparison to that found from the simulation.

There is also some data recorded from the actual event itself, this being a field survey carried out by the French police where they were able to calculate the maximum water elevations at sites around the banks of the valley. This was based on marks left by the receding water on various objects.

The flooded area also included three hydroelectric plants which were situated along the Reyran River. The position of these electrical transformers is known and since the flood impact cause them to turn off, the arrival times of the flood wave is also available.

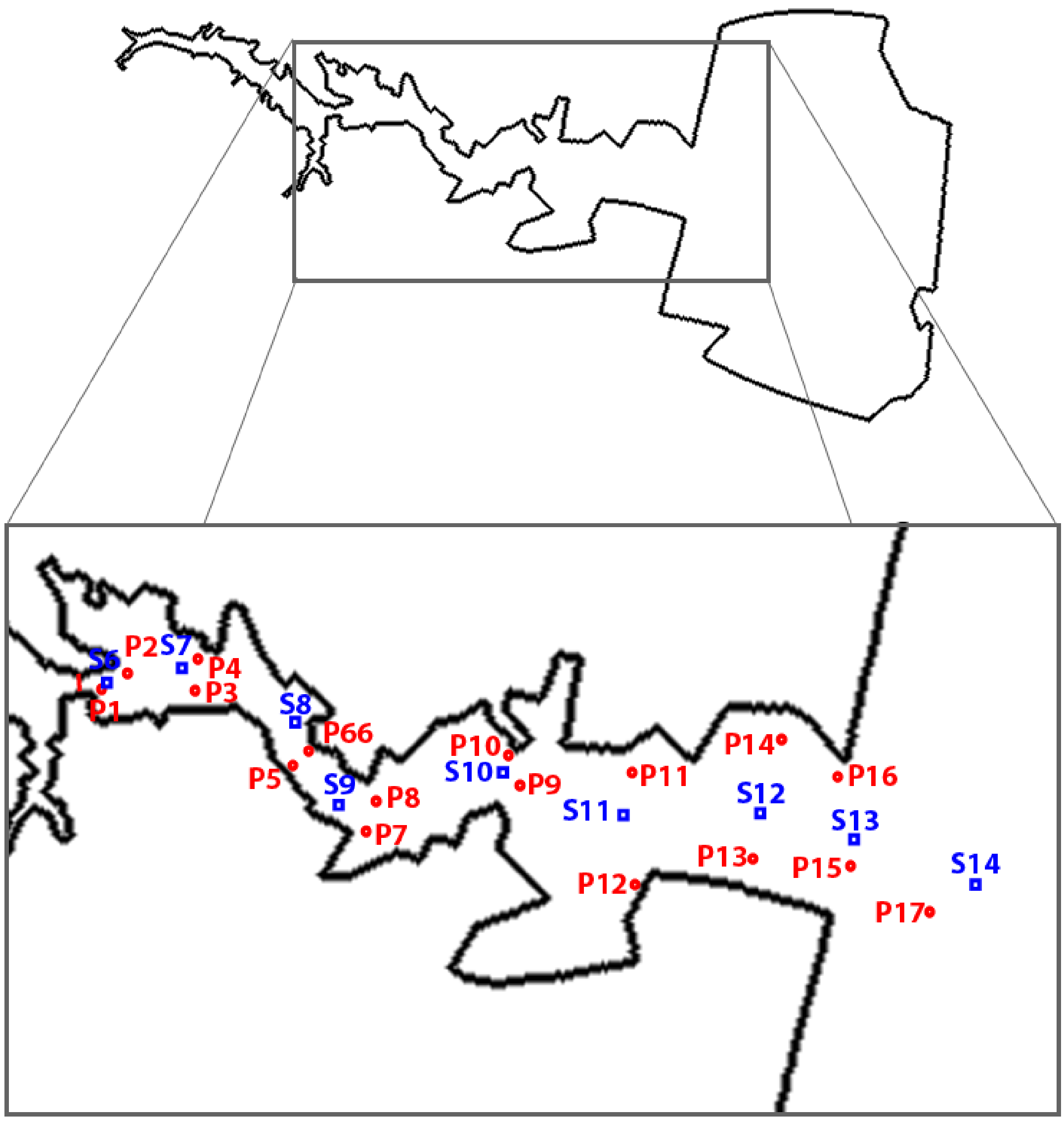

Figure 5: Location of points of comparison with police points from the actual flood in red and points from the scale model in blue

The results can therefore be compared to these sets of existing data. It is important to know that the data does not even exactly agree with each other as the data from the scale model is not completely in line with the observations from the actual dam. Nevertheless, this provides a useful comparison.

The positions of these various point can be seen in Figure 5.

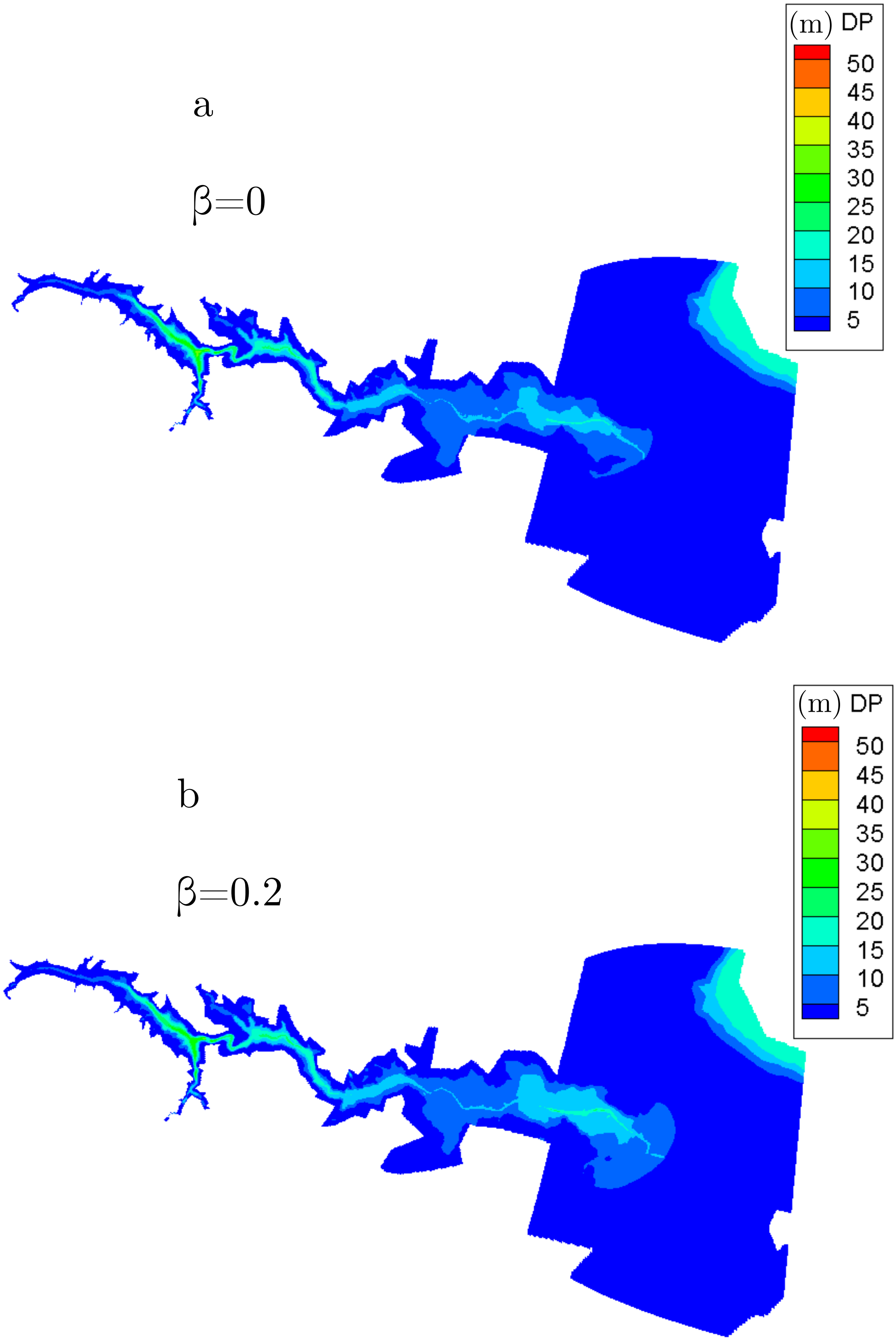

a
β=0
(m) DP
50
45
40
35
30
25
20
15
10
5
b
β=0.2
(m) DP
50
45
40
35
30
25
20
15
10
5

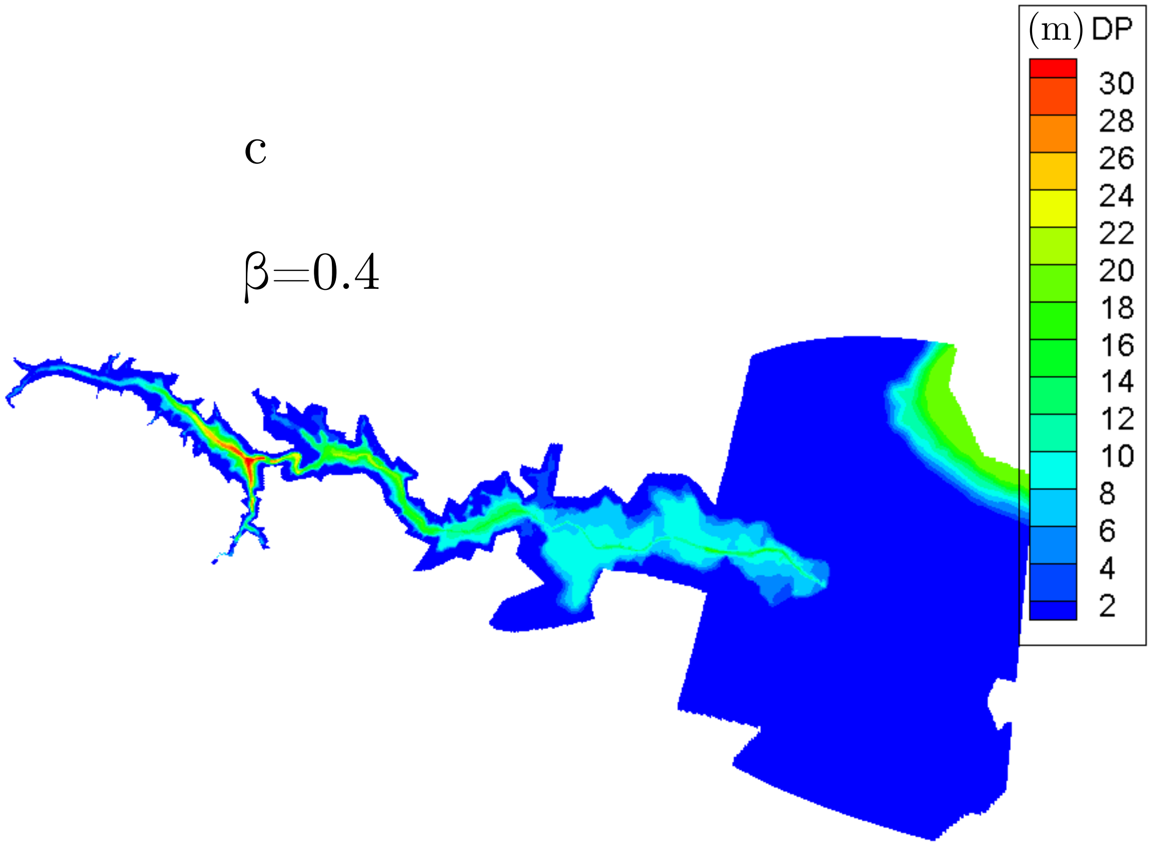
c
β=0.4
(m) DP
30
28
26
24
22
20
18
16
14
12
10
8
6
4
2

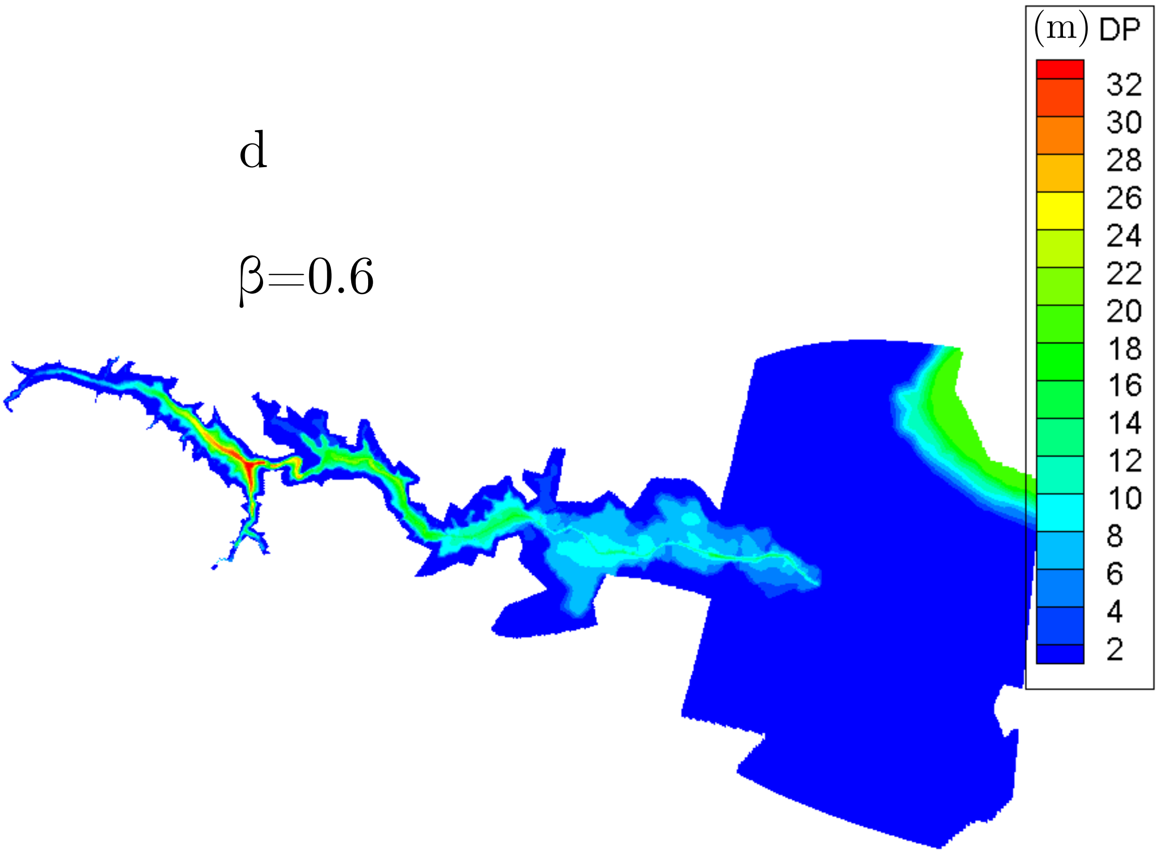
d
β=0.6
(m) DP
32
30
28
26
24
22
20
18
16
14
12
10
8
6
4
2

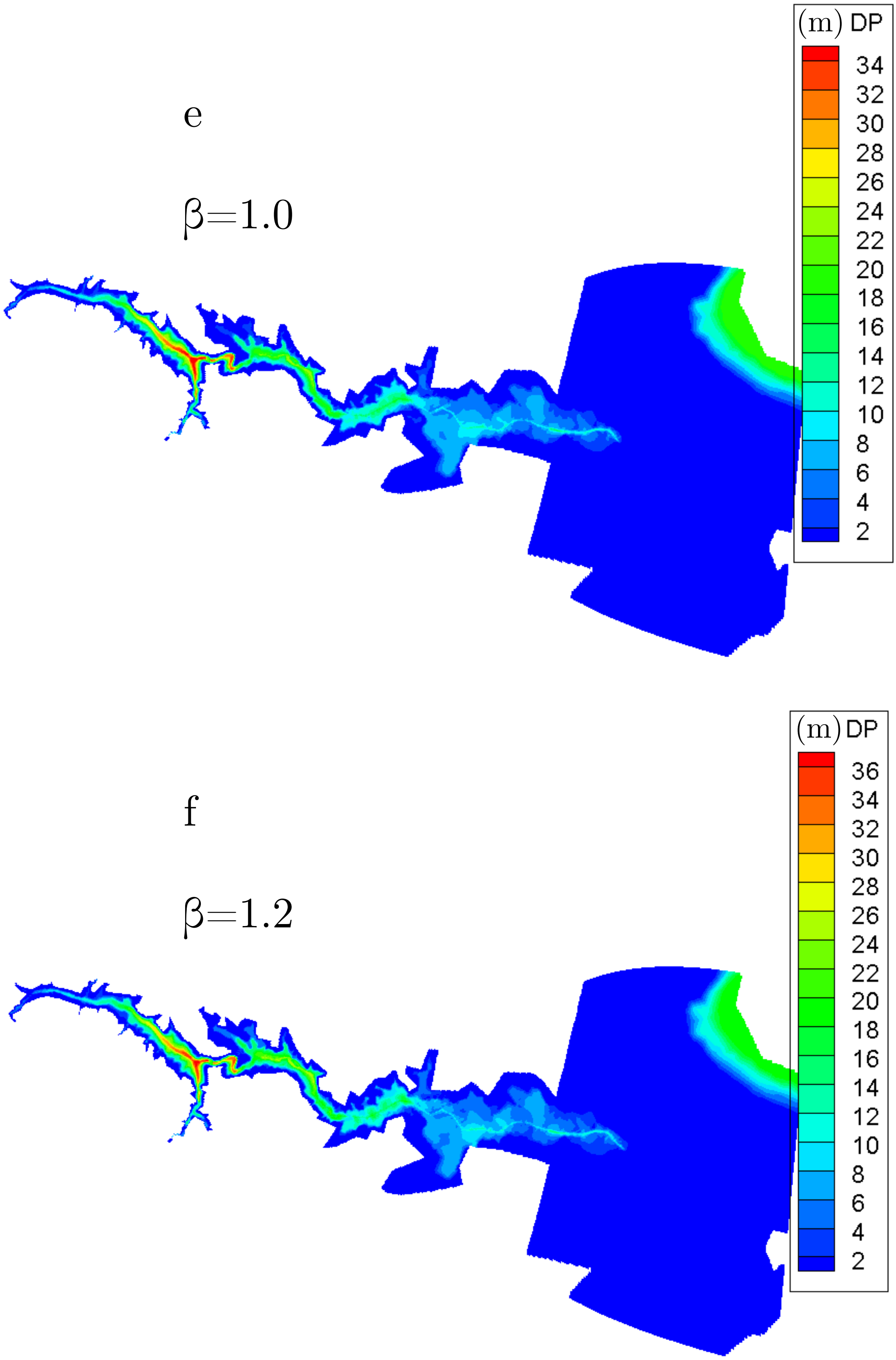

Figure 6: (a – f) A ‘snapshot’ of the water depth (m) 20 minutes after the flood for different values of the Boussinesq coefficient

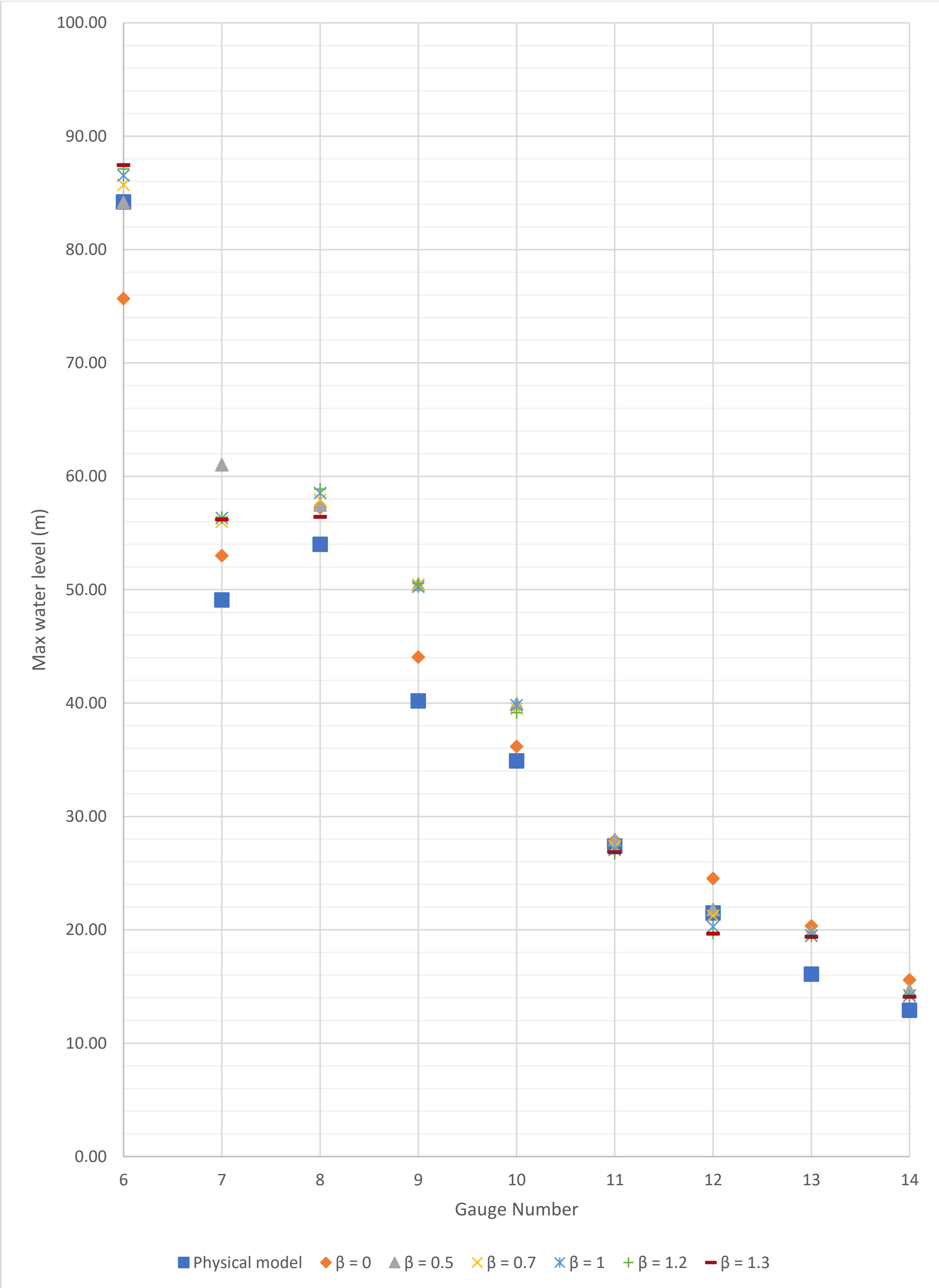

Figure 7: The variation in maximum water level at different gauges in the scale model of the Malpasset Dam for a range of values of the Bousinnesq coefficient

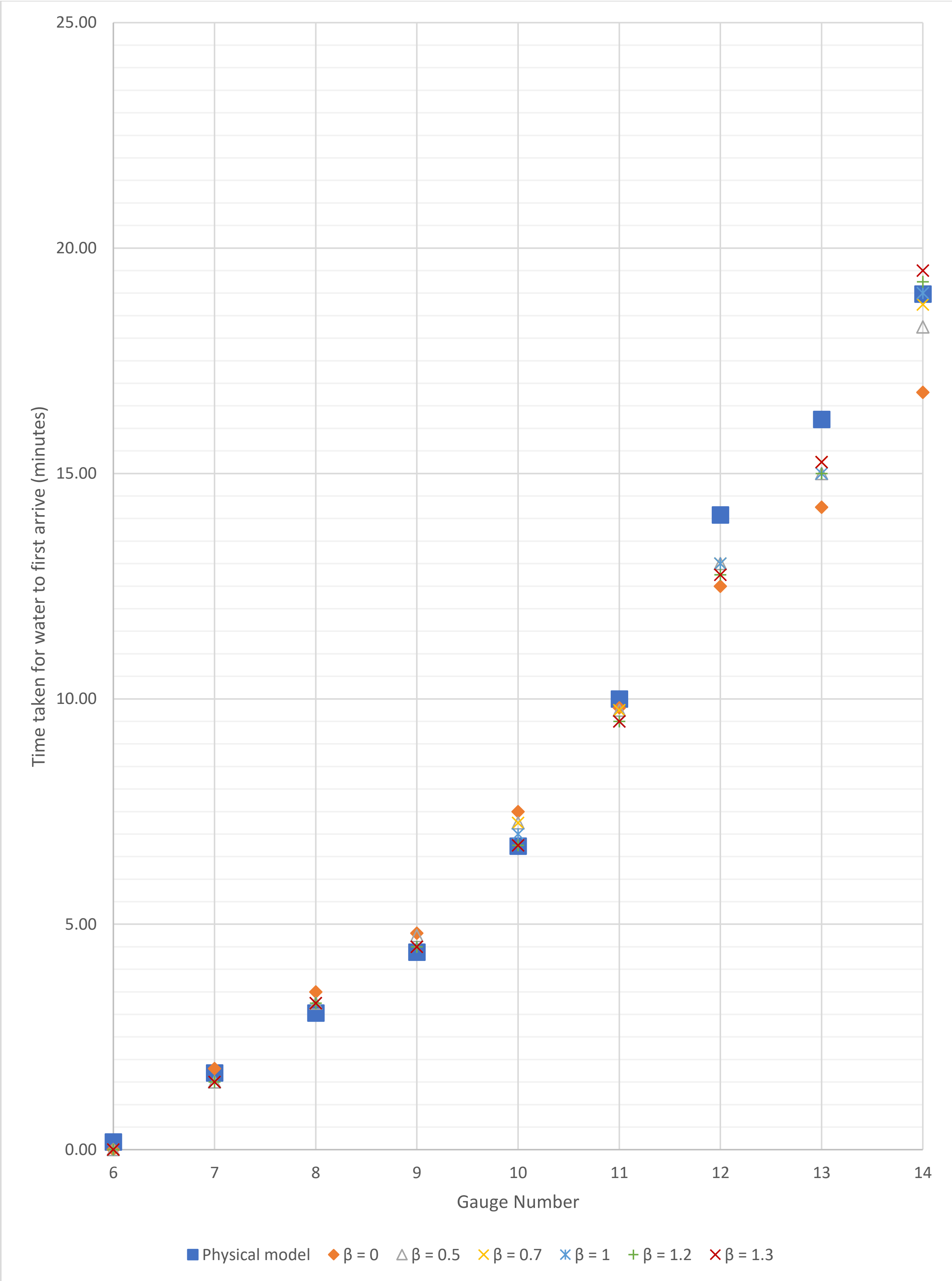

Figure 8: The variation in time of water arrival at different gauges in the scale model of the Malpasset Dam for a range of values of the Bousinnesq coefficient

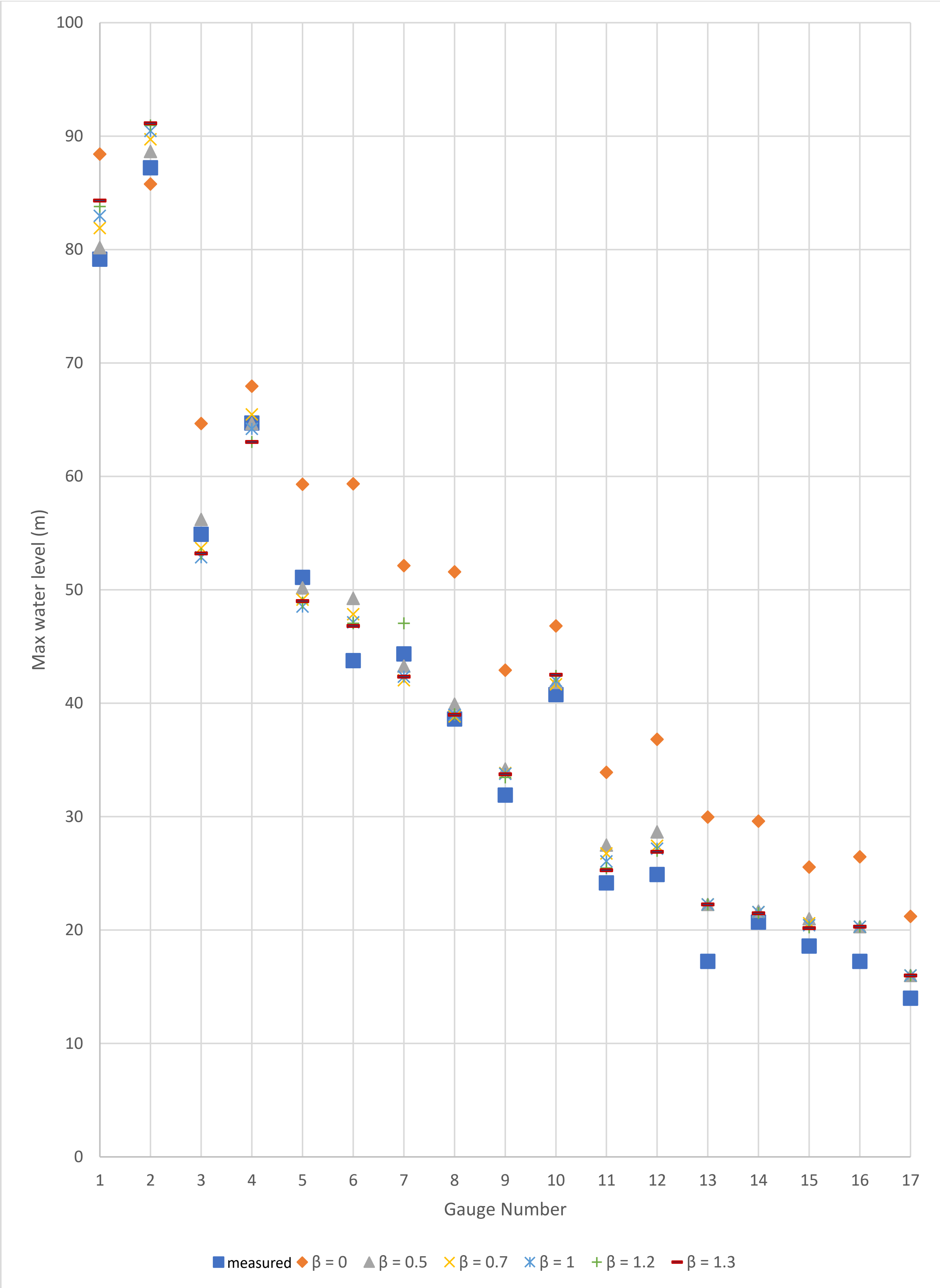

Figure 9: The variation in maximum water level at different points surveyed by the French police for a range of values of the Bousinnesq coefficient

4.2.1 Time series comparison

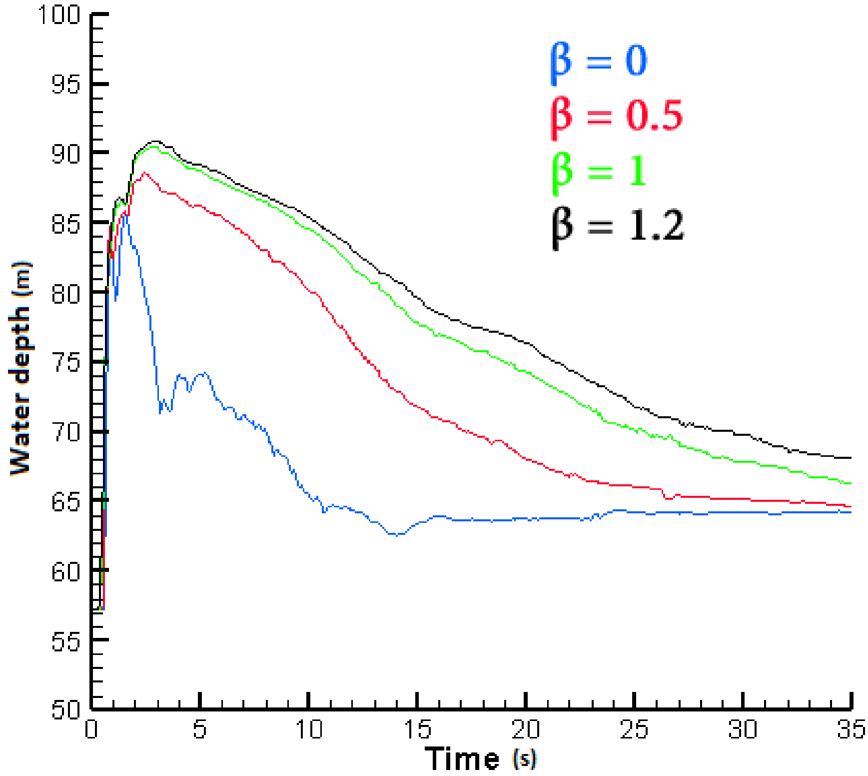

Figure 10: water depth (relative to datum) at point 'P2' over time for different values of the coefficient

4.3 Discussion

4.3.1 Qualitative

In Figure 6 a 'snapshot' of the water depth 20 minutes after the dam break is seen. The full simulation was run up to 30 minutes into the event, but this provides a good visual comparison for the differences observed due to changes in the Bousinnesq coefficient.

The most obvious difference is with the simulation that was done with a value of zero and 0.2 for the coefficient (Figure 6 a and b). The flood wave has advanced significantly more than the other simulations and is spread out over a 'wider' area. In contrast, the tests with larger values of the coefficient show a much smaller wave front that has not advanced as far downstream and is not as wide.

In order to further understand the differences between the results, a macro script was written to extract readings for the locations that correspond to gauge points in the scale model and points where the French police took readings at the time of the flood.

4.3.2 Maximum water levels

Figure 7 shows how the maximum water lever at the different gauges compares to the maximum water level found for the different simulations. There does not seem to be much of a correlation or trend observed but the results show reasonable agreement with each other and all also so closeness to the measured values from the model.

The result for the test with a zero value for the coefficient (therefore a scenario in which momentum is mostly neglected) shows greater discrepancy than the other results and tends to not be ‘grouped’ as close to the remainder of the tests. This would be expected since such a circumstance is highly unusual and does not make any physical sense.

However, it is interesting to see how the results for the test with a zero value for the coefficient, still do not vary much from the readings measured from the model. In order to gain a better understanding of this, the mean absolute difference between the recorded result and measured readings for each value of the coefficient, are graphed in Figure 11.

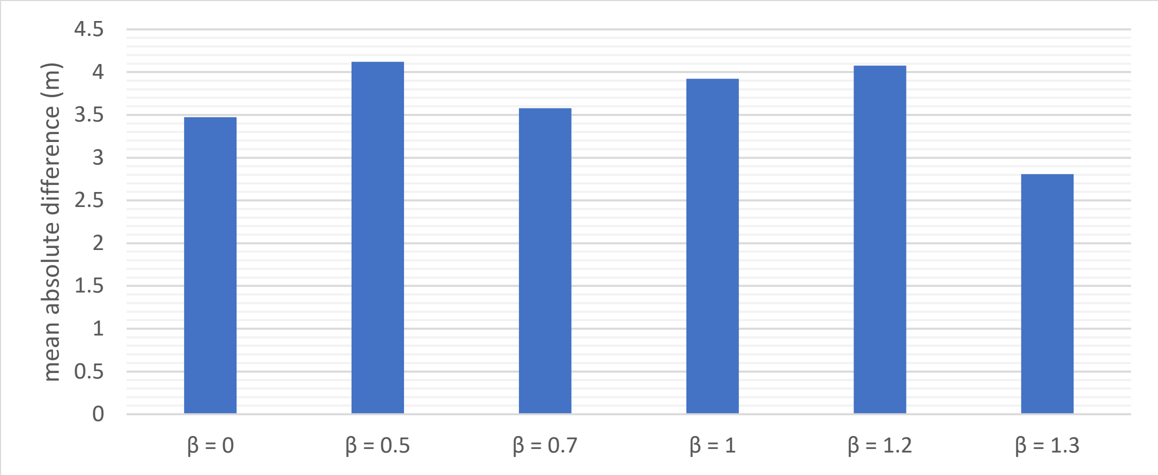

Figure 11: mean absolute difference between the simulated max water level and the max water level from the scale model, for all the gauge points

Since the theoretical and experimentally observed 'correct' value for the Bousinesq coefficient is almost exactly 1, the results for this value would have been expected to show the least difference from the measured readings and therefore be the most accurate. However, this is very clearly not the case and all tests were observed to show similar variation from the experimental values taken from the scale model test.

This suggest that there is no significant effect on the accuracy of maximum water depth predictions due to the choice of Boussinesq coefficient. An alternative explanation could be a systematic error due to the setup of the simulation where the boundary conditions, topography and simulated dam break do not completely agree with the design of the model from which the gauge data is obtained.

The test was initially done with the recommended time step of 0.2 seconds and then repeated with a lower time step (of 0.1 seconds) but the trend remained the same.

The results for the points measured by the French police where then looked at instead and can be seen in Figure 9. Overall, the simulations tended to calculate a higher maximum water level than what was recorded during the actual flooding event. But most of the results still lie relatively close to the measured values at the time.

The measured values taken by the French police could have been incorrectly recorded. Or a more obvious explanation is the crude method through which the pre-flood 1931 topography was digitised for the model (based on a field survey maps which may also not be very accurate).

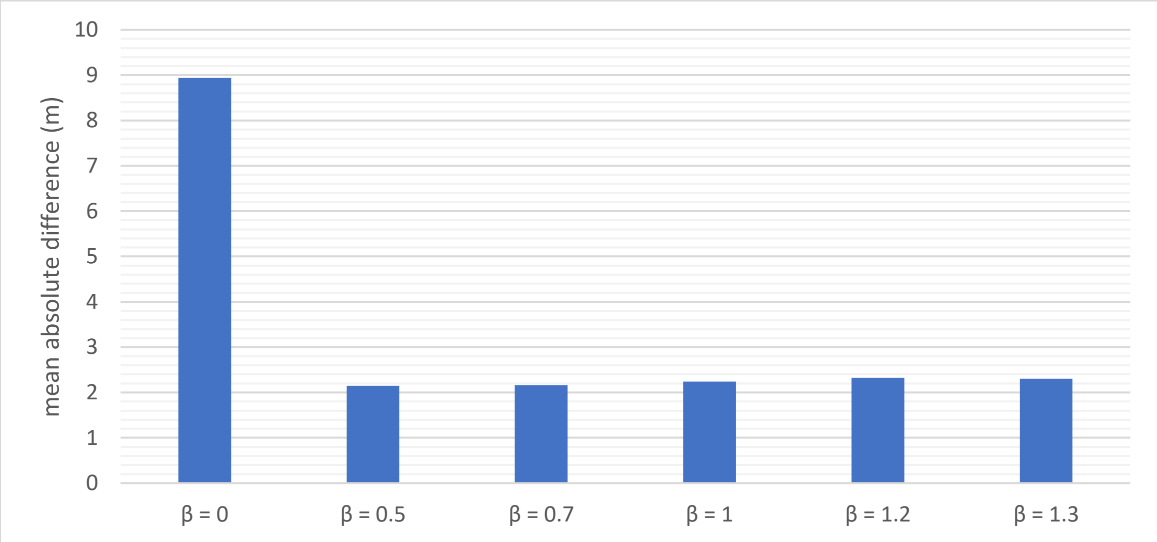

Figure 12: mean absolute difference between the simulated max water level and the max water level measured by the French police after the flood, for all points they measured

The results from the test with a Boussinesq coefficient of 0 being very different when comparing what was found for the gauge points in the scale model test and the data recorded by the French police is notable. There was a much more significant discrepancy for the data at the police points as the simulated maximum water level was much higher than the measured values and also from the remainder of the tests as was seen in Figure 12. This could be explained by the points at which the French police took measurements, were much closer to the 'banks' of the river valley. The points that were placed closer to the 'centre' of the valley and were closer to the points used in the scale model, show less difference between the result when the coefficient is zero and the remaining results. For example, this is seen in points 2 and 4 in Figure 9.

This may suggest that simulations done with a zero value of the Boussinesq coefficient are not accurate for points on the edges of the flood zone. They tend to significantly overestimate the maximum water level compared to the actual level observed or what would be calculated with a more reasonable value used for the coefficient

But for the remainder of the test, there was no significant benefit for using the 'correct' Boussinesq value closer to one and no overall trend was observed to indicate that values closer to one were more accurate at predicting the maximum water depth.

4.3.3 Time for waterfront to arrive

When looking at the data in Figure 8 there is a much clearer trend to be observed. In the near field region, which is further upstream and closer to the Dam, the results for tests with a lower value of the coefficient show more time taken for the water to reach the gauge. This would indicate that the flood wave is not progressing as fast in this region (up to gauge 10).

But the opposite effect is true in the far field region as the river valley becomes wider. The time for the wave front to reach the next four gauges is much lower for the lower Boussinesq value test suggesting that it speeds up. This coincides with the results from larger values of the coefficient (such as for $\beta=1.3$) being much higher indicating a slower moving flood wave. Overall suggesting that lower values of the coefficient result in a faster moving wave in the far field region once the flood wave has spread out, but a slower moving flood wave in the near field closer to the Dam.

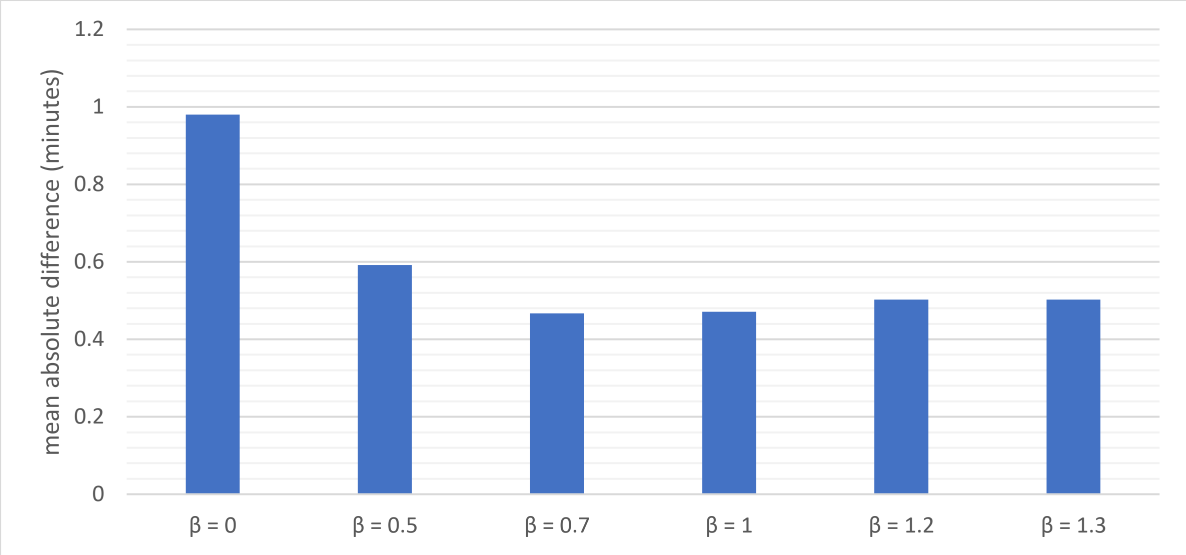

Figure 13: mean absolute difference between the simulated arrival time and the arrival time measured in the scale model test for different values of the coefficient

Like the previous sets of results for maximum water level, the mean absolute difference between the simulated time for the wave front to arrive and for the range of coefficient values tested was calculated and can be seen in Figure 13.

The values of the Boussinesq coefficient closer to the theoretical and experimental value, and therefore closer to 1, show somewhat more significant agreement with the values found in the scale model test. This suggests that the choice of value for the coefficient does have an effect on the accuracy of the simulation when considering how well the propagation time is calculated, even though this was not found to always be the case when considering maximum water level.

5 Toce: Setup, Results and Discussion

5.1 Setup

As with the previous setup, this simulation was done based on a setup from previous research[7]. The European Commission funded a CADAM (Concerted Action on Dambreak Modelling) study which included building a 100:1 scale model of a 5km reach of the Toce River valley in northern Italy. The dimensions of the physical model were 55m x 13m and various gauges were placed in the model to study the extreme flooding event. The model does not include buildings and bridges, but instead increases the ground elevation where they would be present. The topography can be seen in Figure 14 and an interesting feature is the reservoir near the centre of the model. It features a 2% average slope while some areas exceed this greatly which signifies the need for the model to have shock capturing capability.

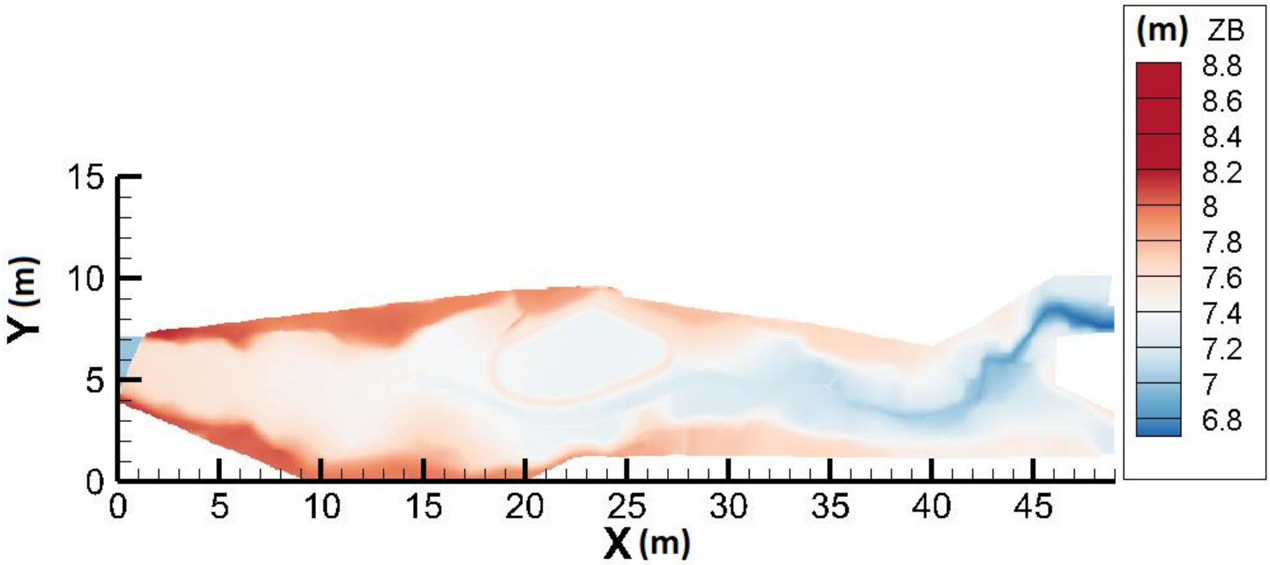

Figure 14: Topography and dimensions of the TOCE river valley model (note: the elevation shown here is the actual elevation while the dimensions are the scaled dimensions from the scaled model)

Unlike the previous test, the grid is orthogonal so a Jacobian transformation is not required, and the formula used in the solver is based on the original non-conservative form of the Boussinesq equations. However, the Mac-TVD finite difference scheme is still being used as was for the Malpasset simulation.

The flow rate from the model test and variances in water level were applied to the 'inlet' of the model. The valley was initially set to be dry at time zero. In this test the minimum prescribed water level for a grid cell to be considered dry in the calculations was set to 0.005m.

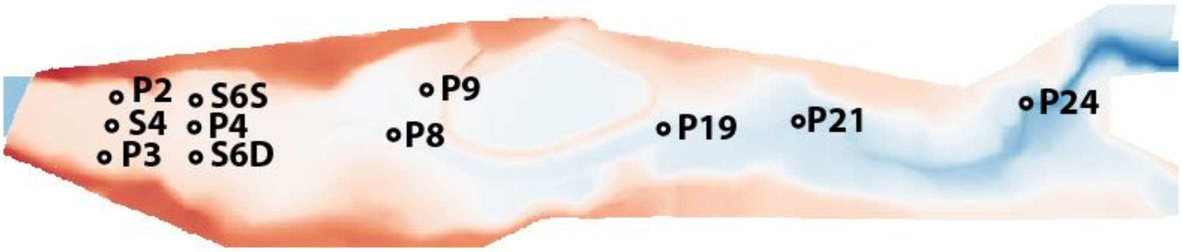

Figure 15: Location of gauge points for which data is available from the scale model of the Toce River Valley

On the right, near the downstream ends, the bed elevation has an abrupt drop resulting in critical flows upstream of the outlets. The boundary condition which is then specified for the outlets should therefore not have any effect on the flow filed observed in the inner domain.

As with the Malpasset model, various gauge points are present in the scale model and their locations have been overlaid on the topography map in Figure 15.

5.2 Results

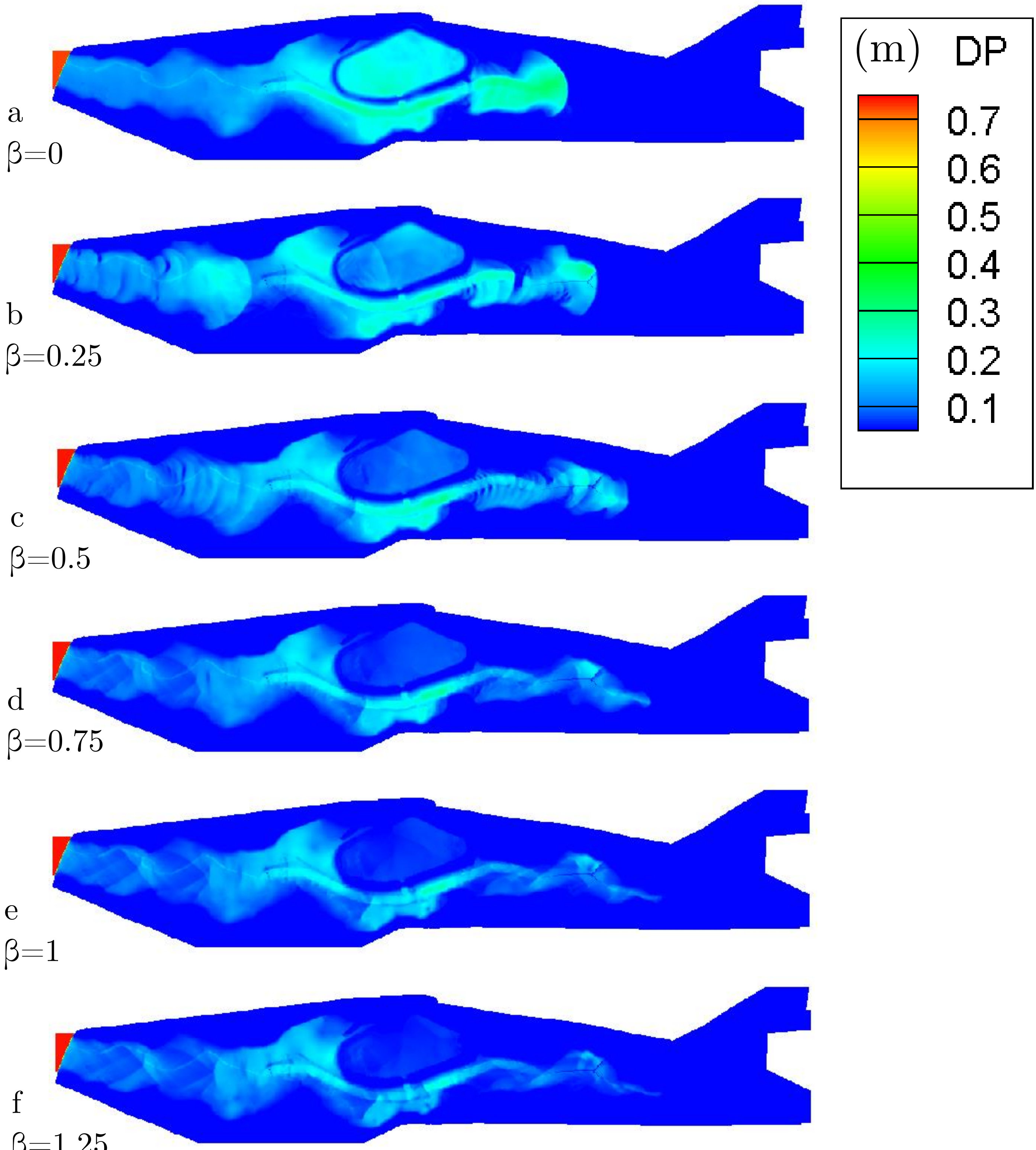

Figure 16: Contour plots of water depth after 500 seconds since the start of the 'flood' for different values of the Boussinesq coefficient

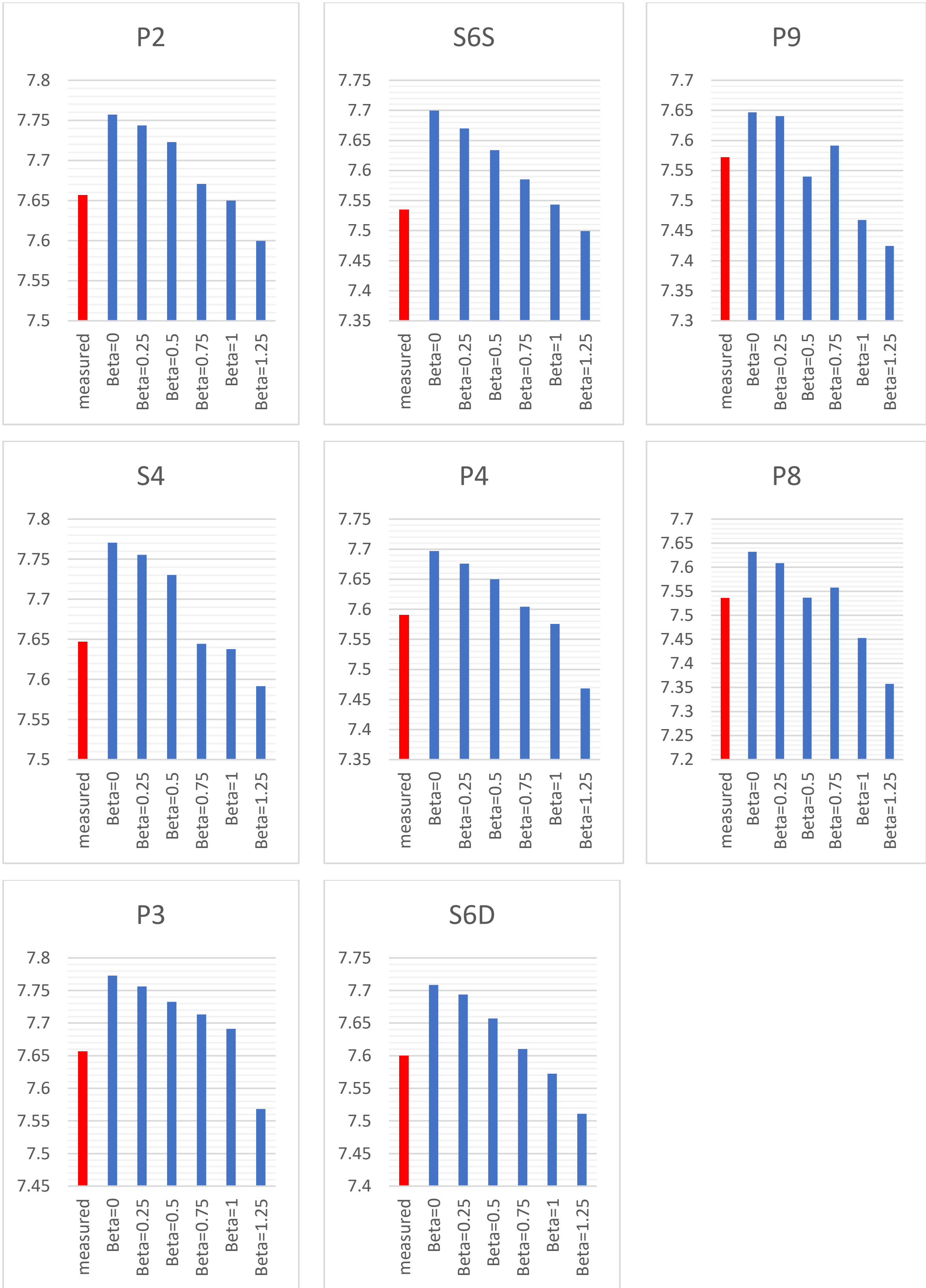

Figure 17: Comparison in maximum water level (m) at different gauges in the scale model of the Toce River valley for a range of values of the Bousinnesq coefficient

Figure 18: Comparison in time for wave front to arrive (minutes) at different gauges in the scale model of the Toce River Valley for a range of values of the Bousinnesq coefficient. Note: data for some of the tests done with a value of 1.25 for the coefficient is not available because the simulation crashed before it reached.

5.3 Discussion

5.3.1 Qualitative

Figure 16 provides a 'snapshot' of the variation in water depth at the same point in time during the simulation. It is clear that there is a general trend of the flood wave having progressed more for lower values of the coefficient and the depth of water also being larger corresponding a greater volume of water having moved downstream. But when comparing the actual distance that the wave has travelled, larger values of the coefficient resulted in a shallower wave that was not as wide but had reached further downstream and was therefore moving faster than the deeper and more spread out wave observed for smaller values.

An interesting feature is how there is more water that managed to overtop the 'reservoir' which is situated near the centre of the model win the tests with a lower Boussinesq coefficient value. This remains the same even when looking at results from later on in the simulation for tests done with higher values of the coefficient. Unfortunately, there is no data present for the water level in the reservoir itself during the scale model test as this would have provided an interesting comparison.

5.3.2 Maximum water levels

A comparison of maximum water levels experienced at the various gauge points is given in Figure 17. There is a very clear trend in these results, lower values of the Boussinesq coefficient result in a higher maximum water level.at the gauges tested. This is very different to the trend (or lack thereof) observed from the Malpasset tests.

There is a slight discrepancy with the result for $\beta=0.75$ at gauges P9 and P8 but the general trend remains the same.

As was done for the previous test cases a comparison between the accuracy of the different test cases can be made by looking at how different they are from the results measured in the physical model.

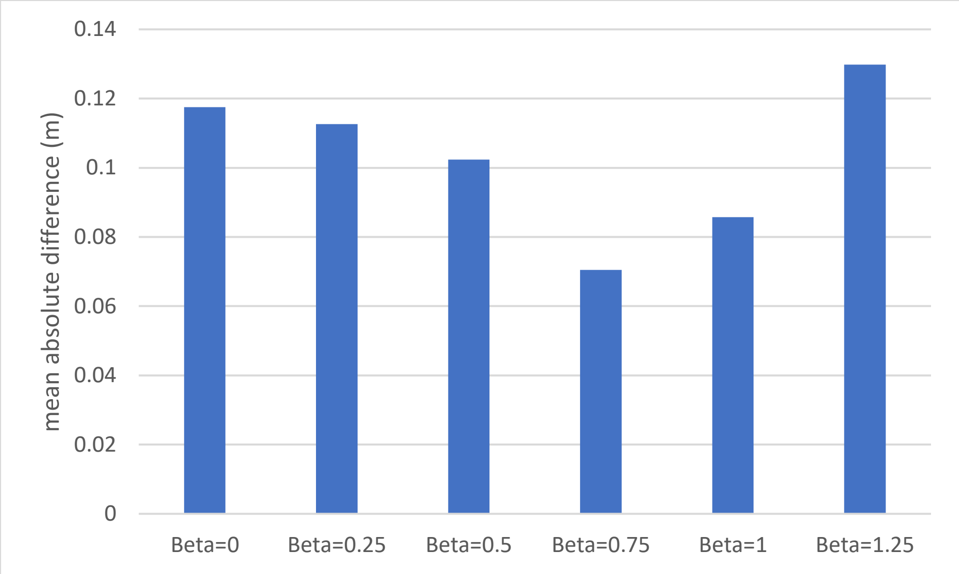

Figure 19: mean absolute difference between the simulated max water level and the max water level measured in the scale model, for all gauge points

As can be seen in Figure 19 there is a trend for extreme values of the coefficient being less accurate or that they do not agree with the data from the scale model as well. But in this case the 'correct' value of the coefficient (1) appears to show less accuracy than the test conducted with a smaller value (0.75). As detailed earlier in the report, the Boussinesq coefficient should not theoretically or experimentally be below one and in most cases, it is very close to unity. This may suggest that there could be discrepancy between the topography used for the scale model and that used in the simulations.

Even so, the results are reasonably close to the others (only about a 10% difference is seen between the two extremes) and do not convey any startling differences. For the Malpasset tests, there was no clear trend indicating certain values of the coefficient being less accurate when compared to the physical data (other than test with a value of 0 being much less accurate when considering the police points). However, this is not seen in this experiment and there is more of a trend with 'extreme' values that are further away from 1 showing more inaccuracy. This would have otherwise been expected and it is interesting for it not to have been seen in the first set of tests.

5.3.3 Time for waterfront to arrive

A comparison of the time taken for the wave front to arrive at the various gauges has been show in Figure 18. In this case the overall trend is extremely clear and followed almost linearly when considering values of the Boussinesq coefficient. As the Boussinesq coefficient is increased, the time taken for the water to reach the chosen points decreases. This corroborates the findings from the contour plots in Figure 16 where this was also observed.

This differs from the results seen in the Malpasset tests as in that case, the opposite trend was true far downstream. This can be easily explained by considering how the simulate Toce River valley is 5km long while the Reyran River valley from the Malpasset experiment is 17km long. And the results from the gauges closer to the upstream end did show the opposite trend in the Malpasset case. Gauge 10 (Figure 5) was the furthest gauge away from the dam to exhibit the same trend as seen for the Toce test. This point is 4.8km away from the dam which is similar to the size of size of the Toce model. This could suggest that the initial flow results in lower values of the coefficient causing the flood wave to propagate much slower while further downstream the opposite is true, and the same would possibly have been observed had the Toce River valley been larger. Instead, it may be that the topographies of the initial section in Malpasset and Toce have similar features that cause this effect.

6 Conclusion

6.1 Main Findings

The tests on two situations that are meant to represent 'real-world' supercritical flows including uneven terrain, showed that the value chosen for the Boussinesq coefficient does not have a very large impact on the predicted flooding. The theoretical, experimental, and most often used value of the coefficient is almost always one. But tests showed that the in some cases when comparing with data from real-life or scale model test floods, the results for simulations done with values for the coefficient as unrealistic as zero or as high as 1.5 still showed reasonable accuracy.

Still, there were some general differences observed. Lower values of the Boussinesq coefficient resulted in flood waves that were slightly 'wider' and deeper. This was especially seen when looking at points that are further away from the 'centre' of the river valleys. And therefore means by increasing the value of the Boussinesq coefficient, the area of inundation is increased.

Another minor difference observed was a change in time taken for the flood waves to reach downstream points. Which corresponds to slower or faster moving flood waves. In relatively upstream regions where the flow is more restricted and the ground features a steeper slope, having a smaller value for the coefficient tends to result in a slower moving wave. However, when looking at regions further downstream that have a more 'flat' topography, this effect is reversed.

Since the water depth is also determined through the flow velocity, due to conservation of mass. This justifies the larger water depths seen for lower values of the coefficient in the Toce tests and the upstream region of the Malpasset tests.

Previous research[13] suggests that for a frictionless bed, increasing the Boussinesq coefficient leads to an overprediction of the propagating speed of the flood wave. This is consistent with what was observed in the upstream/more steep regions. When bed friction is more significant, the opposite effect is observed. When looking the downstream region of the Malpasset test, this would seem to be confirmed.

6.2 Future Work

More tests need to be done with other scenarios that potentially feature more distinct and different topography. This would allow for a greater understanding of at what point the trend of a faster moving wave due to larger Boussinesq coefficient reverses as previously it was seen to occur is the bed friction became significant.

It would also be important to be able to categorize the exact point and by how much bed friction needs to increase for the observed trend to reverse.

A study to quantify the inundated area and how it changes based on the chosen value of the coefficient would also be helpful. This could include a data from a scale model test as reference or from a real-life flood.

7 References

[1] European Environment Agency. (2018). *Reservoirs and dams*. [online] Available at: https://www.eea.europa.eu/archived/archived-content-water-topic/reservoirs-and-dams [Accessed 12 May 2020].

[2] Rawlinson, L. (2019). *In recovery – three weeks on from Whaley Bridge - Creating a better place*. [online] Blog.gov.uk. Available at: https://environmentagency.blog.gov.uk/2019/08/23/in-recovery-three-weeks-on-from-whaley-bridge/ [Accessed 12 May 2020].

[3] Boussinesq, J., 1877. *Rapport Sur Un Mémoire De M. Boussinesq, Présenté Le 28 Octobre 1872 Et Intitulé " Essai Sur La Théorie Des Eaux Courantes "*. Paris: Imprimerie nationale.

[4] Castro-Orgaz, O. and Hager, W.H. (2009). Curved-streamline transitional flow from mild to steep slopes. *Journal of Hydraulic Research*, 47(5), pp.574–584.

[5] Chanson, H. (2004). *Environmental hydraulics of open channel flows*. Amsterdam ; Boston: Elsevier Butterworth Heinemann.

[6] Liang, D., Lin, B. and Falconer, R.A. (2007). A boundary-fitted numerical model for flood routing with shock-capturing capability. *Journal of Hydrology*, 332(3–4), pp.477–486.

[7] Liang, D., Lin, B. and Falconer, R.A. (2007b). Simulation of rapidly varying flow using an efficient TVD–MacCormack scheme. *International Journal for Numerical Methods in Fluids*, 53(5), pp.811–826.

[8] Ying, X., Jorgeson, J. and Wang, S.S.Y. (2009). Modeling Dam-Break Flows Using Finite Volume Method on Unstructured Grid. *Engineering Applications of Computational Fluid Mechanics*, 3(2), pp.184–194.

[9] Bellier, J., 1967. *Le barrage de Malpasset*. Editions Science et Industrie.

[10] Testa G. (ed.). Third CADAM Meeting Proceedings. Milan: Italy, 1999

[11] Valocchi, A.J. and Malmstead, M. (1992). Accuracy of operator splitting for advection-dispersion-reaction problems. *Water Resources Research*, 28(5), pp.1471–1476.

[12] Nujić, M. (1995). Efficient implementation of non-oscillatory schemes for the computation of free-surface flows. *Journal of Hydraulic Research*, 33(1), pp.101–111.

[13] Yang, F., Liang, D. and Xiao, Y. (2018). Influence of Boussinesq coefficient on depth-averaged modelling of rapid flows. *Journal of Hydrology*, 559, pp.909–919.

[14] Goldstein, S., 1938. Modern Developments in Fluid Dynamics, vol. 1. Oxford University Press, England.

[15] Flood Modeller. (2019). *Flood Modeller*. [online] Available at: https://www.floodmodeller.com/ [Accessed 26 May 2020].

8 Appendix

8.1 Health and Safety

As stated in the risk assessment form, this project was entirely computational. As discussed in the assessment, the only risks were related to the amount of computer work. And the precautions which were laid out in the report, such as taking breaks were adhered to and risks mitigated.

8.2 Acknowledgements

I would like to express my very great appreciation to Dr Liang for supervising this project.